Rotation-Variant Template Matching for Supervised Hyperspectral Boundary Detection

Harald van der Werff, Frank van Ruitenbeek, Mark van der Meijde, Freek van der Meer, Steven de Jong, and Saman Kalubandara

***Abstract*—Edge operators are widely used on gray-level images and are recently improved to work with multispectral and even hyperspectral imagery. The high spectral information content in hyperspectral images allows a detailed description of boundaries and thus a supervised boundary detection. In this letter, we describe a template matching algorithm for the detection of fuzzy and crisp boundaries. For this purpose, the template has a one-dimensional design consisting of two different spectra. This template is matched to a remote sensing image by moving and rotating the template over the image. A statistical spatial and spectral fit of the template is calculated for every position and orientation. Important steps in this approach are the design of a template according to our knowledge of a boundary, and, mainly depending on the template design, the interpretation of the algorithm output. The algorithm has been used for the detection of boundaries between selected mineral assemblages in a hyperspectral image that covers a hydrothermal alteration system. Results show that the algorithm successfully detects the boundaries that had been defined in the templates. In addition, it is shown that rotation of the template in the algorithm reveals information on the type of boundary (crisp or fuzzy) and identifies pixels where only one of the template endmembers is present.**

***Index Terms*—Edge detection, spatial, spectral, supervised, template matching.**

I. Introduction

DETECTION of boundaries by edge operators is widely applied to gray-level or low-dimensional images. Recently, edge operators have been extended from gray-level images to multispectral and hyperspectral imagery [1]. The high spectral information content in hyperspectral images allows a detailed description of boundaries and favors the use of a supervised boundary detection algorithm. A boundary in an image is defined by the existence of at least two spectrally or texturally contrasting areas, and can as such be described by an image template. This letter presents a "rotation-variant template-matching" (RTM) algorithm for the supervised detection of boundaries in a hyperspectral image.

Template matching is a pattern recognition technique that is widely used for detection of objects in gray-level images [2]. In the past, it has been applied for machine vision such as optical character recognition, face detection, object detection, and defect detection [3]. In this letter, a template is a miniature image, consisting of 3×1 pixels, that contain information of a boundary between two spectrally contrasting pixels. The template is moved over the image like a moving kernel. At every position, the template is rotated, and a statistical fit is calculated for every pose (Fig. 1).

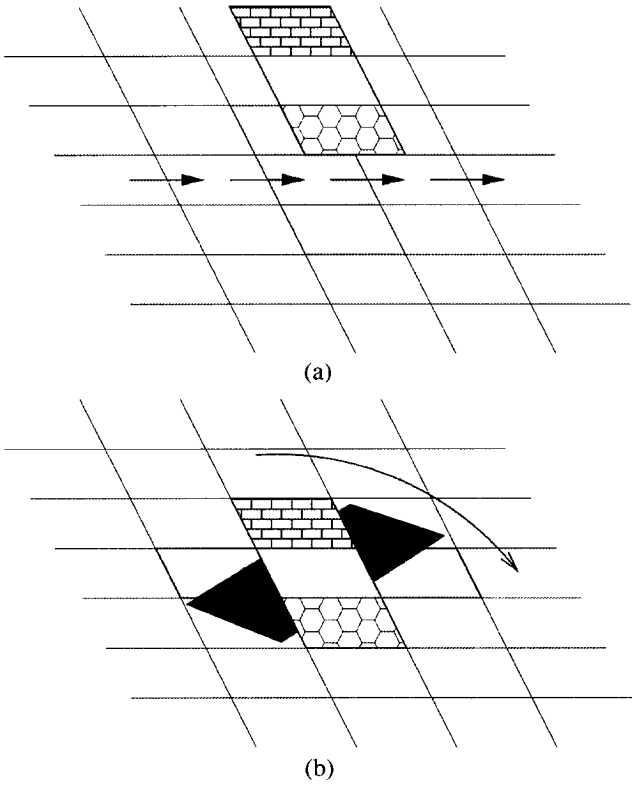

Fig. 1. Template is matched by (a) moving it over an image and (b) changing the template orientation at every position by 45° increments up to a total of eight orientations.

Usually, rotation invariance is a desirable and therefore an often studied feature in template matching [4], as conventional spatial cross-correlation algorithms cannot be applied when an object can be rotated [5]. However, the variance in spectral fit of the template, obtained by fitting at different orientations, contains pertinent information that can be used for interpretation of the spectral signature of an object. Our algorithm has consequently been designed to be rotational variant.

The RTM algorithm is applied to synthetic data to clarify and evaluate the algorithm output. Next, the algorithm is applied

Manuscript received December 23, 2005; revised April 12, 2006.

H. van der Werff, F. van Ruitenbeek, M. van der Meijde, and F. van der Meer are with the International Institute for Geo-information Science and Earth Observation (ITC), 7500AA Enschede, The Netherlands (e-mail: vdwerff@itc.nl).

S. de Jong is with the Faculty of Geosciences, Utrecht University, NL-3508 Utrecht, The Netherlands.

S. Kalubandara is with the Geological Survey and Mines Bureau, Dehiwala, Sri Lanka.

Color versions of one or more of the figures in this paper are available online at http://ieeexplore.ieee.org.

Digital Object Identifier 10.1109/LGRS.2006.886424

1545-598X/$25.00 © 2007 IEEE

to a hyperspectral image that covers a hydrothermal alteration system in southeastern Spain, with the aim of detecting boundaries between specific mineral assemblages in this system.

II. RTM Algorithm

The spectral fit (F_p) between each template pixel and its respective image pixel can be expressed by a spectral angle [6]. Other distance measures in feature space could however be used alternatively, depending on which measure is most suitable for matching the spectral information in a template to an image. Following [1], the spectral angle between the two vectors $\vec{v}$ and $\vec{w}$, which stand for a template and an image spectrum, is calculated as

$$F_p = SA(\vec{v}, \vec{w}) = \cos^{-1}\left(\frac{\vec{w}\cdot\vec{w}}{\|\vec{v}\|\,\|\vec{w}\|}\right). \quad (1)$$

The "spectral fit" of the entire template (F_s) is the mean spectral fit of all template pixels:

$$F_s = \frac{\sum_{p=0}^{N} F_{(p)}}{N} \quad (2)$$

where N is the number of template pixels. The variance in spectral fit of all template pixels ("spectral variance," V_s) is for every position and orientation of the template calculated as

$$V_s = \frac{\sum_{p=0}^{N}\left(F_{(p)} - F_s\right)^2}{N}. \quad (3)$$

At each position, the best fit of the template found by rotating is saved as "optimal fit" (F_{opt}). As we use a 3 × 1 template in our research, a 45° increment with a total of eight template orientations (A) is sufficient not to miss an optimal template orientation. The "rotation variance" (V_r) is calculated as

$$V_r = \frac{\sum_{a=0}^{A}\left(F_{s(a)} - F_r\right)^2}{A} \quad (4)$$

where $F_s(a)$ is the spectral fit for template orientation a and F_r is the mean F_s of A rotations. The measures F_{opt} and V_r, obtained by (2) and (4), respectively, contain only spatial information of the template fit. To additionally acquire information on the spectral fit of a template, the initial spectral fit obtained with (2) and (3) is summarized and saved as "mean spectral variance" ($\overline{V}_s$):

$$\overline{V}_s = \frac{\sum_{a=0}^{A} V_{s(a)}}{A}. \quad (5)$$

In total, we extract three measures from the algorithm: F_{opt}, V_r, and $\overline{V}_s$. We limited the algorithm to odd template dimensions with the consequence that a template always has a center pixel. This simplifies the calculation of pixel coordinates when rotating a template, and the location of the image pixel that coincides with the center pixel of the template can be used to save the RTM algorithm output. The value of the center pixel itself is ignored. This allows a crisp boundary, which theoretically would fall in between two image pixels, to be indicated in the algorithm output image by a double-pixel line centered around the theoretical position of the boundary.

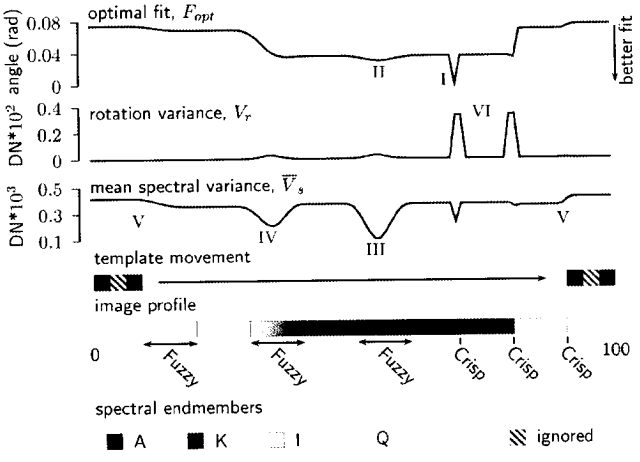

Fig. 2. RTM profiles obtained by matching a 3 × 1 template with a spectrum of kaolinite (K) and alunite (A) to an artificial hyperspectral image with fuzzy and crisp boundaries between pixels with pure spectra of kaolinite (K), alunite (A), illite (I), and quartz (Q).

III. Application to a Synthetic Image

For mapping a boundary between two spectrally contrasting areas, we need to know that both spectral signatures that have been defined in the template are present. In case either signature is found to be present, we also need to know whether these signatures form a crisp boundary or an intrapixel mixture, thereby coexisting or forming a fuzzy boundary. F_{opt} will have a high match in case both template endmembers are present and a low match in case none of the template endmembers is present. V_r indicates the presence or absence of a crisp boundary and will be relatively low when the template match is similar for all orientations, which happens when none of the spectral signatures are found or when both are present as a mixture. The measure V_r will be relatively high when at least one of the spectral signatures is found and forms a crisp boundary. Spectrally pure pixels can be distinguished from the mixed pixels by a relatively high $\overline{V}_s$, as the difference in spectral fit between the pixels will be maximal for these locations.

To support these hypotheses, a simple experiment has been done by matching a 3×1 template with spectra of pure kaolinite (K) and alunite (A) to an artificial image (Fig. 2). The artificial image is 100 pixels wide and has, from left to right, three fuzzy boundaries of 10 pixels wide and three crisp boundaries. The areas marked with A, K, I, or Q, respectively, consist of pure spectra of kaolinite, alunite, illite, and quartz and are 10 pixels wide. F_p was determined by the vector angle between image and template pixel [6]. F_{opt} is consequently expressed as vector angle, meaning that a low value represents a good template fit and vice versa. The template fit is optimal for the crisp boundary A K (I in Fig. 2), and respectively decreases for the fuzzy boundary A K (II), presence of only A or K and absence of minerals A and K (in areas I and Q). $\overline{V}_s$ has the lowest values for fuzzy boundary A K (III), with an increase for fuzzy boundary K I (IV) and high values for both boundaries between areas I and Q (V). The combination of a high $\overline{V}_s$ and F_{opt} in areas A and K can be used to differentiate between areas in which only one signature can be found and areas that have a mixture of both signatures. The graph of V_r in

TABLE I
SENSITIVITY[1] OF RTM MEASURES TO TYPE OF BOUNDARY AND NUMBER OF ENDMEMBERS

Endmembers present	*Two*		*One*		
Type of boundary	*Fuzzy*	*Crisp*	*Fuzzy*	*Crisp*	*None*
F_{opt}	+	+	±	±	±
V_r	±	+	±	+	−
$\overline{V_s}$	+	±	+	−	±

[1] + = high, ± = moderate and − = none

Fig. 2 has high values for crisp boundaries involving only one or both signatures (VI), lower values for fuzzy boundaries and relatively low values for boundaries where none of the template signatures can be found. Table I summarizes the results of Fig. 2 and shows that a combination of the measures F_{opt}, V_{r}, and $\overline{V}_{\text{s}}$ allows the detection of a boundary between two spectrally contrasting areas.

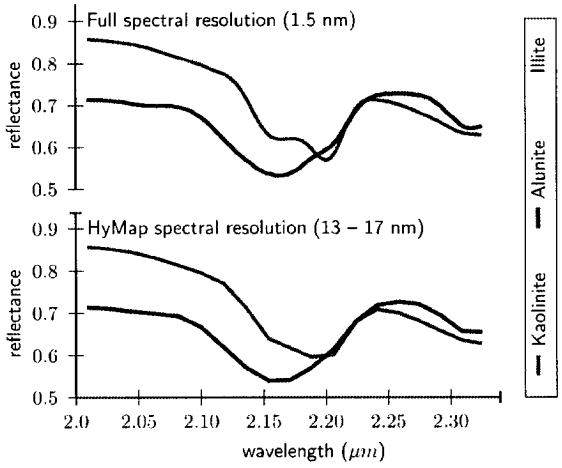

Fig. 3. SWIR spectra of alunite (dark gray), kaolinite (gray), and illite (light gray) from the JPL spectral library [7] at full resolution (top) and at HyMap resolution (bottom).

IV. APPLICATION TO A HYPERSPECTRAL IMAGE

The RTM algorithm has been applied to a HyMap hyperspectral image [8] acquired over the Rodalquilar caldera complex in southeastern Spain during the HyEurope campaign in July 2003 [9]. The Rodalquilar caldera complex consists of two nested calderas that were formed by volcanic eruptions about 11 Ma ago [10]. After the lower parts were subsequently covered by lake and lacustrine sediments, the caldera complex underwent an intensive epithermal alteration that resulted in two alteration systems: the Cinto system and the Los Tollos system [11]. Five alteration types can be differentiated in zones around the area of maximum alteration [11]. Ranging from highest to lowest alteration intensity, these zones are silicic, advanced argillic, intermediate argillic, sericitic, and propylitic. A simplified geological model of the Los Tollos alteration system has quartz and alunite in the center, surrounded by a halo of dominantly kaolinite, which, in its turn, is surrounded by a halo with enrichment of illite.

The 250 × 250 pixels subset of the HyMap image covers the Los Tollos alteration system. The image was atmospherically corrected by the German Aerospace Center (DLR) with the Atcor4 package [12] and was delivered in reflectance values. As the third spectrometer (1.4–1.8 μm) had not recorded any data on this flight, the distinctive absorption feature for alunite at 1760 nm could not be used. The image was spectrally subsetted to 19 short wavelength infrared (SWIR) bands (2009–2325 nm) to include only the wavelengths containing diagnostic absorption features for kaolinite, alunite and illite and, consequently, to avoid possible interference of other nondistinctive spectral features.

Two 3 × 1 templates with mineral combinations kaolinite–alunite and kaolinite–illite were created from JPL laboratory spectra [7] after resampling to the spectral resolution of HyMap. At HyMap resolution, the differences between these spectra can mainly be found in the position of the broad main absorption band of each mineral, as the distinctive double absorption feature of kaolinite is affected by the resampling to the Hymap resolution (Fig. 3). The vector or spectral angle [6] was chosen as spectral matching method because this method is not sensitive to brightness differences between library spectra and image spectra [1].

V. RESULTS

The algorithm results are shown as images in Fig. 4. Fig. 4(a) shows that V_{r} detects crisp boundaries between alunite and kaolinite in the center of the image (cyan), while crisp boundaries between illite and kaolinite are detected northwest of the center (red). These results are in agreement with Fig. 4(b), which shows semi-abundances of alunite, kaolinite, and illite by means of an inverted color composite of rule images obtained with a spectral angle classification. The boundaries are also visible in red tones in Fig. 4(c) and (d), which show RGB color composites of V_{r}, F_{opt}, and $\overline{V}_{\text{s}}$ for the templates kaolinite–illite and kaolinite–alunite, respectively. As previously stated in Fig. 2, pixels with mixtures of the template spectra have a relatively high F_{opt} and therefore a relatively narrow vector angle. Consequently, the black tones in Fig. 4(c) and (d) indicate a good fit of the template while green tones indicate a wide vector angle and thus a marginal fit. The areas indicated as having kaolinite–illite coexistence are more abundant northwest of the center [Fig. 4(c)] when compared to the areas of kaolinite–alunite coexistence which are mainly abundant in the center of the image [Fig. 4(d)]. The deep blue areas in Fig. 4(c) and (d) have a relative high value for mean template variance, which, following the results of Fig. 2, indicates the presence of only one of the minerals. Template matching results obtained with a single template do not indicate which of the signatures is actually found.

Profiles of the template matching results have been extracted over the entire width of the image at a northing of 4080208 (UTM zone 30N), indicated by the East–West striking white line in Fig. 4(b). Fig. 5 compares the RTM profiles to a mineralogical profile that shows dominant abundances of alunite, kaolinite, or illite. This mineralogical profile has been interpreted from a spectral angle classification of the HyMap image using the resampled spectra of alunite, kaolinite, and illite (Fig. 3). This interpretation was assisted by a profile of

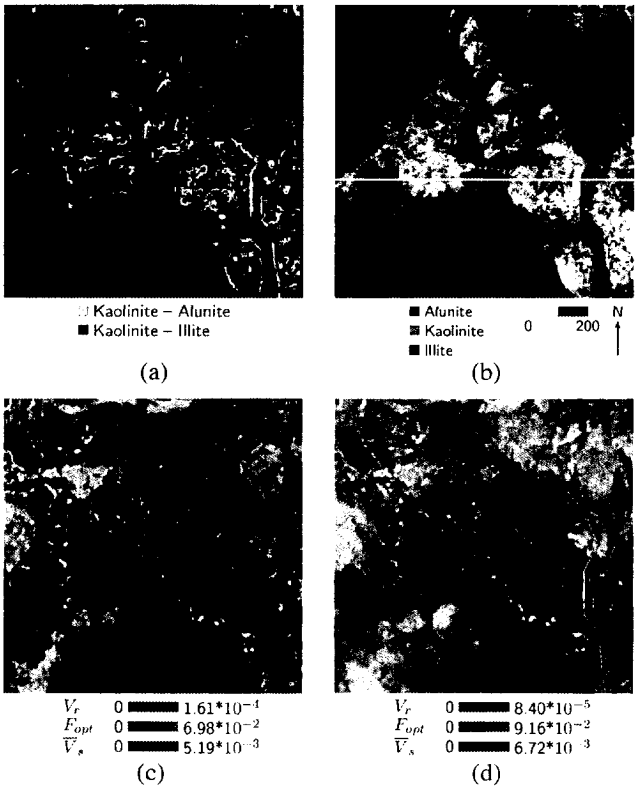

Fig. 4. RTM results for detection of crisp boundaries. (a) Rotation variance of both templates, clearly showing crisp alunite–kaolinite boundaries in the center (cyan) and crisp kaolinite–illite boundaries in the north and northwest (red). (b) Inverted color composite of gray-level images showing a degree of similarity based on the spectral angle. This image is interpreted as relative abundances of the respective minerals. The white East–West striking line in (b) indicates the location of the profiles in Fig. 5. The white asterisks indicate locations of ASD field spectral measurements. RTM results for detection of crisp and fuzzy boundaries. (c) and (d) show the rotation variance (red), optimal template fit (green), and mean spectral variance (blue) for a kaolinite–illite and kaolinite–alunite template, respectively.

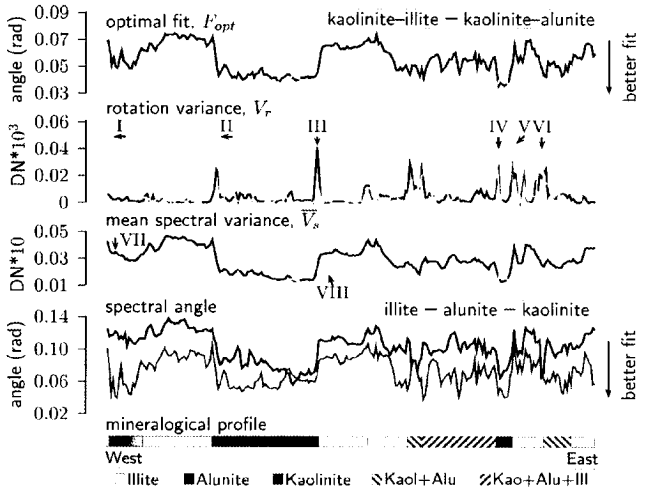

Fig. 5. Profiles of the Spectral Angle Mapper results of Fig. 4(b) and the RTM measures of Fig. 4(c) and (d). This figure shows from top to bottom the F_{opt}, rotation variance, mean spectral variance, and the spectral angle. The mineralogical profile at the bottom was interpreted from the "spectral angle mapper" classification using resampled spectra of pure alunite, kaolinite, and illite. Field reflectance measurements have been used to interpret the spectral mixture, while the locations of boundaries are interpreted from the displayed SAM profiles. The dashed areas in the mineralogical profile have frequent changes in mineralogy and result in the frequent occurrence of peaks in the eastern part of the RTM profiles.

ASD Fieldspec measurements acquired every 20 m along a 1.2-km long transect in the Los Tollos area in June 2004.

The graph for F_{opt} in Fig. 5 shows, in agreement with the mineralogical profile, a few large jumps in the Western part of the profile (for example as indicated by I, II, and III). The Eastern part, which has frequent changes in mineral abundances, has accordingly a dozen smaller jumps (for example IV, V, and VI). The jumps in the graph for F_{opt} can be recognized as peaks in the graph for V_{r}. Points I, II, IV, V, and VI show crisp boundaries between kaolinite and illite, and III, IV, V, and VI show crisp boundaries of kaolinite and alunite. While most of the peaks are unique for one template (such as I, II, and III), the values for peaks IV, V, and VI are for both templates in the same range. These three double peaks are likely to be a result of man-made crisp boundaries between alunite and illite: The area between V and VI is a valley with a road. The area between IV and V is an open pit alunite mine, which can be also seen in the F_{opt} profile for kaolinite–alunite and the spectral profiles of Fig. 5. The graphs for $\overline{V}_{\text{s}}$ resemble the graphs for F_{opt} to a large extent. Although the transect covers only a few areas where one of the endmembers is present, the deviations that result in the bluish tones in Fig. 4 can be seen in Fig. 5. Points VII and VIII are examples of a deviation between the graphs for $\overline{V}_{\text{s}}$ and F_{opt} which are slightly higher than the average differences between the graphs. However, like the image results for $\overline{V}_{\text{s}}$, the profiles also do not indicate which endmember is present.

VI. Discussion

Fig. 4 shows that the RTM algorithm can detect the selected crisp boundaries between mineral assemblages. Additionally, Fig. 4(c) and (d) shows that the rotation of the template provides an additional information by making a distinction between crisp boundaries (red tones), areas with mineral coexistence (black tones), areas where one endmember is dominant (deep blue tones), and areas where the template has a marginal fit (pale green tones). These results show that the RTM technique is a valuable tool for preparation of mineral maps, e.g., prior to a fieldwork.

The results in Fig. 4 and in Section III show that the application of a 3 × 1 template can simultaneously detect crisp as well as fuzzy boundaries. An application of longer templates, e.g., 5 × 1 pixels, is likely to favor the detection of crisp boundaries between homogeneous areas at the cost of detection of wide boundaries. At the same time, a longer template with a margin that is not evaluated, e.g., the three center pixels of a 5 × 1 template, favors the detection of wide boundaries. Lengthening templates consequently involves a more accurate description of the type of boundary that is to be detected.

Although the RTM algorithm was designed for boundary detection and not for mapping areas with a homogeneous mineralogy, a combination of several template matching results can provide a sufficient information to identify which mineral is present in areas with a relative high $\overline{V}_{\text{s}}$. The results of a standard spectral angle classification in Fig. 4(b) show that the bluish areas in Fig. 4(c) are rich in illite, while

the bluish areas in Fig. 4(d) are rich in kaolinite (or depleted from illite and alunite). As alunite is only present together with kaolinite, the bluish areas in Fig. 4(c) that are pale green in Fig. 4(d) can be classified as illite and the bluish areas in Fig. 4(d) that are pale green in Fig. 4(c) can be classified as kaolinite.

Spectral confusion can possibly result from three different causes. The first cause is inconsistencies between the image spectra and the laboratory spectra used in the template. Image spectra are influenced by the atmosphere and illumination of the sun, while the laboratory spectra have been measured in controlled conditions with artificial light on pure and grinded rock samples. Still, the RTM algorithm only indicates a relative and not an absolute fit of a template and should be relatively insensitive to these spectral inconsistencies, unless the different spectra have a different sensitivity to inconsistencies. This is, however, a general problem in remote sensing and not a drawback of the RTM algorithm solely. A second cause is an overlap between areas with kaolinite–alunite and kaolinite–illite mixed pixels, as shown by the measure F_{opt} in Fig. 4(c) and (d) (in green). This is caused by the presence of kaolinite in the central alunite zone as well as the gradual increase of illite in the direction of the outer zones. A third cause is that kaolinite is not only spatially located between the alunite-rich and illite-rich zones: The dominant absorption features of kaolinite are, especially at HyMap resolution, located in between the absorption features of alunite and illite (Fig. 3). This spectral confusion in the detection of the fuzzy boundaries of kaolinite–alunite and kaolinite–illite may lead to a spatial confusion.

The RTM algorithm is, as opposed to pixel-based classifiers, a computing intensive algorithm. Although technically speaking, there is no preference in which the method to apply to do a spectral interpretation of an image, it may be clear that the kind of knowledge that a user requires for applying a template matching algorithm is very different from the kind of knowledge needed for traditional mapping algorithms. While a traditional mapping requires knowledge on spectral behavior of the studied area and all targets that make up an object, the RTM technique mainly requires (nonspectral) expert knowledge of the studied object itself and a thorough interpretation of the algorithm results.

A future application lies in the support of traditional algorithms to improve hard classification results. Hard classifications are usually obtained by thresholding of gray-level images of a soft classification. The user that determines the threshold is required to have a detailed knowledge of an area or an object in order to get an adequate mapping result. Although it is possible to gain this information from the field, a consequence is that remote sensing images rarely give new information to a user and that results tend to be scene specific. The RTM results could enhance the thresholding used in pixel-based algorithms. For mapping of mineralogical zonations, rule images could be thresholded by limiting the spatial extent of an object to the boundaries indicated by the RTM algorithm, and as such, by changing from scene specific to object specific, provides new information from an image.

Future development lies in making the RTM algorithm completely scene generic. This would require the algorithm output, which is now relative to the selected measure of spectral fit, to be normalized or, even better, standardized. Another interesting future development is to make use of the sense of direction that is given by the template orientation.

VII. Conclusion

In this letter, we introduced the RTM algorithm for the detection of boundaries in hyperspectral imagery. A novelty in this algorithm is the use of rotation variance in interpreting the spectral signal. The RTM algorithm has been applied to a synthetic image for interpretation of the case-specific output, and has been used for the detection of boundaries between mineral assemblages in a hydrothermal alteration system. The approach was successful in detecting the boundaries as defined in the templates. In addition, the algorithm could indicate the type of boundary (crisp or fuzzy) as well as areas where both or only one of the endmembers is present. The spatial information obtained by rotation of the template is a key factor for the interpretation of the detected boundaries between mineral assemblages. The results of this letter show that the template matching technique is a promising technique in hyperspectral remote sensing. Future development and the use of the algorithm can be in support of pixel-based mapping methods, make use of the direction of sense given by the templates and the application of the algorithm to other research areas.

References

[1] W. Bakker and K. Schmidt, "Hyperspectral edge filtering for measuring homogeneity of surface cover types," *ISPRS J. Photogramm. Remote Sens.*, vol. 56, no. 4, pp. 246–256, Jul. 2002.

[2] D.-M. Tsai and C.-H. Chiang, "Rotation-invariant pattern matching using wavelet decomposition," *Pattern Recognit. Lett.*, vol. 23, no. 1–3, pp. 191–201, Jan. 2002.

[3] D.-M. Tsai and C.-H. Yang, "A quantile-quantile plot based pattern matching for defect detection," *Pattern Recognit. Lett.*, vol. 26, no. 1–3, pp. 1948–1962, Oct. 2005.

[4] F. Ullah and S. Kaneko, "Using orientation codes for rotation-invariant template matching," *Pattern Recognit.*, vol. 37, no. 2, pp. 201–209, Feb. 2004.

[5] M. Choi and W. Kim, "A novel two stage template matching method for rotation and illumination invariance," *Pattern Recognit.*, vol. 35, no. 1, pp. 119–129, Jan. 2002.

[6] F. Kruse, A. Letkoff, J. Boardmann, K. Heidebrecht, A. Shapiro, P. Barloon, and A. Goetz, "The spectral image processing system (SIPS)—Interactive visualization and analysis of imaging spectrometer data," *Remote Sens. Environ.*, vol. 44, no. 2–3, pp. 145–163, 1993.

[7] C. Grove, S. Hook, and E. Paylor, *Laboratory Reflectance Spectra for 160 Minerals 0.4–2.5 Micrometers*, vol. 92-2. Pasadena, CA: JPL Publication, 1992.

[8] T. Cocks, R. Jenssen, A. Stewart, I. Wilson, and T. Shields, "The HyMap airborne hyperspectral sensor: The system, calibration and performance," in *Proc. 1st EARSeL Workshop Imaging Spectroscopy*, M. Schaepmann, D. Schläpfer, and K. Itten, Eds, Oct. 1998, pp. 37–42.

[9] S. Holzwarth, A. Müller, M. Habermeyer, R. Richter, A. Hausold, S. Thiemann, and P. Strobl, "HySens—DAIS7915/ROSIS imaging spectrometers at DLR," in *Proc. 3rd EARSeL Workshop Imaging Spectroscopy*, M. Habermeyer, A. Müller, and S. Holzwarth, Eds, May 2003, pp. 3–14.

[10] J. Rytuba, A. Arribas, Jr., C. Cunningham, E. McKee, M. Podwysocki, J. Smith, W. Kelly, and A. Arribas, "Mineralized and unmineralized calderas in Spain; Part II, evolution of the Rodalquilar caldera complex and associated gold-alunite deposits," *Miner. Depos.*, vol. 25, no. 1, pp. S29–S35, Dec. 1990.

[11] A. Arribas, Jr., C. Cunningham, J. Rytuba, R. Rye, W. Kelly, M. Podwysocki, E. McKee, and R. Tosdal, "Geology, geochronology, fluid inclusions and isotope geochemistry of the Rodalquilar gold alunite deposit, Spain," *Econ. Geol.*, vol. 90, no. 4, pp. 795–822, Jul. 1995.

[12] R. Richter, A. Müller, and U. Heiden, "Aspects of operational atmospheric correction of hyperspectral imagery," *Int. J. Remote Sens.*, vol. 23, no. 1, pp. 145–157, Jan. 2002.